Progress In Electromagnetics Research, PIER 34, 165–187, 2001

ANALYSIS OF AN H-SHAPED PATCH ANTENNA BY USING THE FDTD METHOD

S.-C. Gao, L.-W. Li, M.-S. Leong, and T.-S. Yeo

Department of Electrical and Computer Engineering
National University of Singapore
10 Kent Ridge Crescent, Singapore 119260

Abstract—In this paper, the characteristics of a small antenna using an H-shaped microstrip patch are studied. Significant reduction of antenna size can be realized when the H-shaped patch is used instead of the conventional rectangular microstrip patch antenna. The theoretical analysis is carried out based on the finite-difference time-domain (FDTD) method. The FDTD programs are developed and validated by available measurement results. The effects of various antenna parameters on the resonant frequency and radiation patterns are shown. Several design curves are presented, which are useful for practical antenna design. The electric current distributions on the patch and those on the ground plane are described, together with the results illustrating the electric field distributions under the patch. This antenna is suitable for applications where small size and broad beamwidth are required.

1. INTRODUCTION

Nowadays, due to their several key advantages over conventional wire and metallic antennas, microstrip antennas have been used for many applications, such as Direct Broadcasting Satellite (DBS) Systems, mobile communications, Global Positioning System (GPS) and various radar systems [1–7]. Their advantages include low profile, light weight, low cost, ease of fabrication and integration with RF devices, etc. They can also be made conformal to mounting structures. However, when they are applied in the frequency range below 2 GHz, the sizes of conventional rectangular microstrip patches seem to be too large, which makes it difficult for them to be installed on televisions, notebook computers or other hand-held terminals, etc. Several techniques have thus been proposed to reduce the sizes of conventional half-wavelength microstrip patch antennas. In [8], using high dielectric constant material has been proposed, however, this will lead to high cost and high loss due to the use of high dielectric constant material. Also, poor efficiency due to surface wave excitation is another drawback of this method. Another technique for reducing the size of a microstrip antenna is to terminate one of the radiating edges with a short circuit [4]. The short circuit can be in the form of a metal clampor a series of shorting pins. In [9–12], shorting pins were used in different arrangements to reduce the overall size of the printed antennas. It was shown that by changing the number of shorting pins and the relative positions of these pins, the resonant frequency of the short-circuited microstrip patch can be adjusted. Significant size reduction of microstrip patch antenna has been achieved by using a single shorting pin located near the feed point. One problem with this method is the difficulty in fabrication, as shorting pins have to be accurately inserted into the substrate in specific positions. This difficulty becomes more obvious especially for antenna arrays. Recently, small folded patch antennas without a shorting wall/pin have been proposed [13, 14]. This kind of antenna also demonstrates the capability of size reduction.

Other methods, which involve the modifications of patch shapes have also been proposed. Small microstrip patch antennas using square or rectangular slot loading have been proposed and studied [15–17]. The ring antenna is a special case of slot-loaded microstrip antennas and has been studied by several authors [18]. An H-shaped microstrip patch antenna was firstly proposed in [19]. Experimental results presented in [19] show that the H-shaped microstrip patch has a much smaller size than those of conventional half-wavelength rectangular patch antennas and ring antennas. For practical design purposes, more information about this kind of antenna is required, and

a parametric study based on the full-wave method is needed, which are the motivations of present paper.

The organization of this paper is as follows: Section 2 presents the finite-difference time-domain (FDTD) method used for numerical analysis, and comparisons between theoretical results and experimental results are shown; Section 3 presents a parameter study illustrating the effects of various antenna parameters on the resonant frequency and radiation pattern characteristics, and the electric field distribution under the patch, current distributions on both the patch and the ground plane are also given and discussed; and the paper ends with conclusions in Section 4.

2. ANALYSIS OF H-SHAPED PATCH ANTENNA USING FDTD METHOD

The H-shaped microstrip antenna consists of an H-shaped patch, supported on a grounded dielectric sheet of thickness h and dielectric constant ε_r. The physical dimensions of the H-shaped microstrip patch antenna are shown in Figure 1. The patch has a total length of a. It can be divided into three parts: a center conductor strip with length s and width d, and two identical conductor strips with length w and width b on both sides. The feed point is located at the point (x_0, y_0).

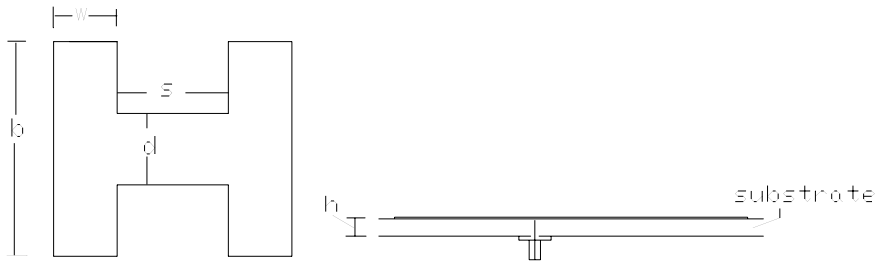

(a) H-shaped patch (b) side view

Figure 1. Configurations of the H-shaped patch antenna.

2.1. Outline of the FDTD Method

In the theoretical analysis, we use the finite-difference time-domain (FDTD) algorithm, because it is very simple to understand and can be used to analyze antennas of many complex structures. As the detailed theory on FDTD is available in [20–24], only a brief outline will be presented here. The first step in designing an antenna with an

FDTD code is to grid up the object. A number of parameters must be considered in order for the code to work successfully. The grid size must be small enough so that the fields are sampled sufficiently to ensure accuracy. Once the grid size is chosen, the time step is determined such that numerical instabilities are avoided, according to the courant stability condition.

A Gaussian pulse voltage with unit amplitude, given by

$$V(t) = e^{-\frac{(t-t_0)^2}{T^2}} \tag{1}$$

where T denotes the period and t_0 identifies the center time, is excited in the probe feed. For the feed probe, we use a series resistor R_s with the voltage generator to model the current in the feed probe [17, 24]. To truncate the infinite space, a combination of the Liao's third-order absorbing boundary conditions (ABC) and the super-absorbing technique is applied, as in [5–6, 17, 21–23]. After the final time-domain results are obtained, the current and voltage are transformed to those in the Fourier domain. The input impedance of the antenna is then obtained from

$$Z_{in} = \frac{V(f)}{I(f)} - R_s \tag{2}$$

To get the electric current distributions on the patch and the ground plane, a sinusoidal excitation at the probe feed is used, which is given by

$$V(t) = \sin 2\pi f_0 t \tag{3}$$

where f_0 is the resonant frequency of interest. The field distributions are recorded at one instant of time after the steady state has been reached. In our analysis, the total time for stability is more than 6 cycles. The electric current distributions J_x and J_y on the metals are obtained by the difference between the tangential magnetic fields above and below the metal interface [17, 24]. After the field distribution has been obtained, the radiation pattern can be readily calculated by using the near-field to far-field transformation [17, 24].

2.2. Comparisons between Calculated and Measured Results

Based on the FDTD algorithm described before, a software package in Fortran 77 language has been developed by us. To verify correctness of the FDTD code, we did a lot of simulations and comparisons are made between many sets of theoretical results and measured results available. Generally, we observe a fairly good agreement among these results. Here, due to limited space, only two examples are shown.

Firstly, the reflection coefficient of an edge-fed rectangular patch antenna is calculated. The patch has a length of 16.0 mm and a width of 12.448 mm. The substrate has a height of 0.794 mm and a relative permittivity of 2.2. The results calculated using present FDTD code and the results measured in [25] are compared in Figure 2(a). In general, the measurement confirms the theory over the entire frequency band. Slight discrepancies between the results are observed, which may be due to numerical errors and the measurement inaccuracies, etc. Two resonance phenomena are shown clearly at 7.6 GHz and 18.3 GHz respectively, just as expected.

In the second example, we calculate the input impedance of the H-shaped patch antenna with the same dimensions as those presented in [19]. The parameters are: $b = 33\,\text{mm}$, $w = 14.25\,\text{mm}$, $s = 26\,\text{mm}$, $d = 15\,\text{mm}$, $\varepsilon_r = 2.5$, $h = 1.59\,\text{mm}$. The calculated results and measured results in [19] are compared in Figure 2(b). Again, a good agreement is observed between them. From these comparisons, we gain confidence in the present FDTD code. It has been concluded in [19] that for the resonant frequency considered, the size of the H-shaped patch is nearly half of the conventional rectangular patch antenna, i.e., a large size reduction can be achieved. In the following, a parameter study of the H-shaped patch antenna is performed using the FDTD code.

3. A PARAMETRIC STUDY OF THE *H*-SHAPED PATCH ANTENNA

3.1. Resonant Frequency

A lot of numerical simulations have been performed by us. It is found that the center conductor strip width d affects the resonant frequency of the H-shaped antenna significantly. Based on numerical results, the variation of resonant frequency versus different values of center strip width d is presented in Figure 3. Resonant frequency decreases according to the decrease in the center strip width d. In this calculation, other parameters of the H-shaped patch antenna are fixed as: $b = 33\,\text{mm}$, $w = 14.3\,\text{mm}$, $s = 26\,\text{mm}$, $\varepsilon_r = 2.5$, $h = 1.59\,\text{mm}$. When d is 33 mm (a conventional rectangular patch), it reaches 1.74 GHz; and 1.14 GHz when $d = 10\,\text{mm}$. The resonant frequency is 0.75 GHz when d is 2 mm. This means a resonant frequency reduction of 57.5% (hence the patch length reduction of 57.5%) compared to the case of the conventional rectangular patch ($d = 33\,\text{mm}$). Thus, it is concluded that the reduction of the center strip width d is a very effective way for effectively reducing antenna size.

Figure 4 shows the characteristics of resonant frequency with respect to the center strip length s. The resonant frequency decreases

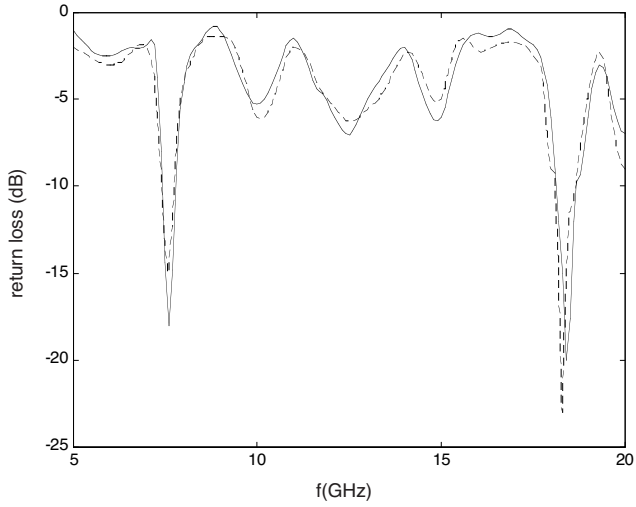

(a) Comparison with measured results in [25]
measured: solid line; calculated: dashed line

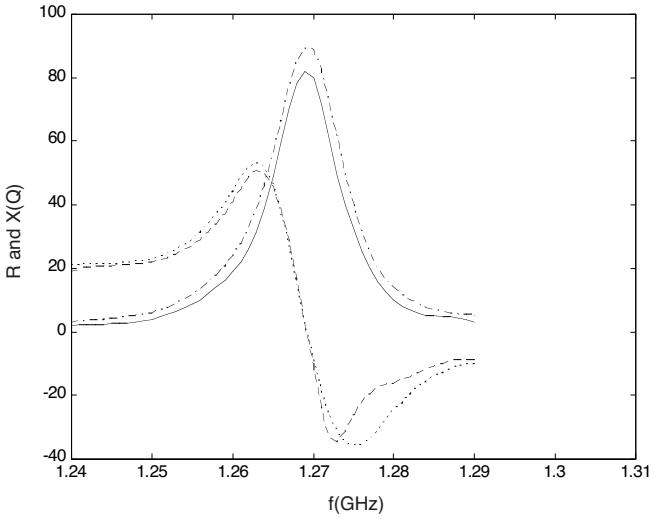

(b) Comparison with measured results in [19]
R calculated: dashed line; R measured: solid line;
X calculated: dotted line; X measured: dashed line

Figure 2. Comparisons between calculated results and measured results.

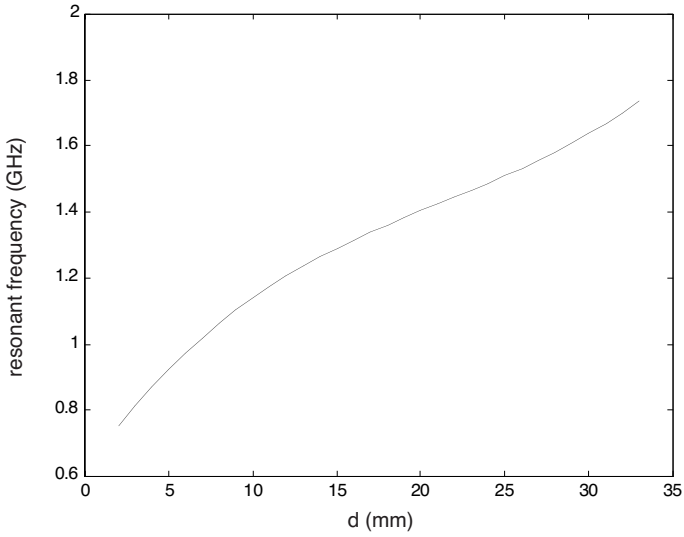

Figure 3. Variation of resonant frequency versus different values of the center strip width.

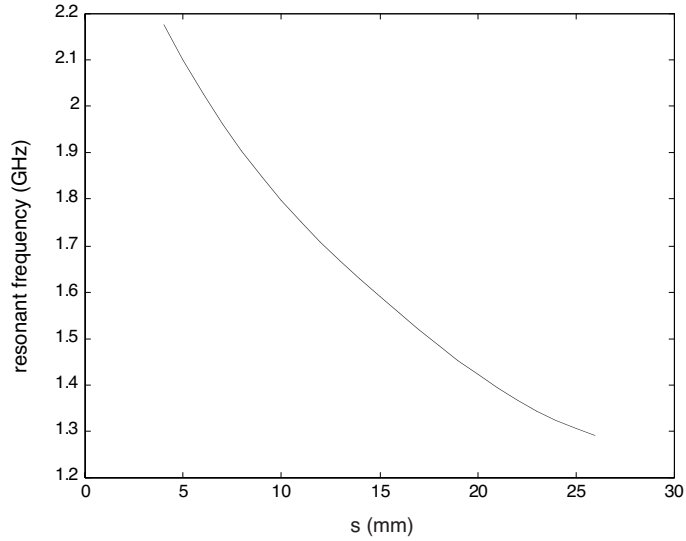

Figure 4. Variation of resonant frequency versus different values of the center strip length.

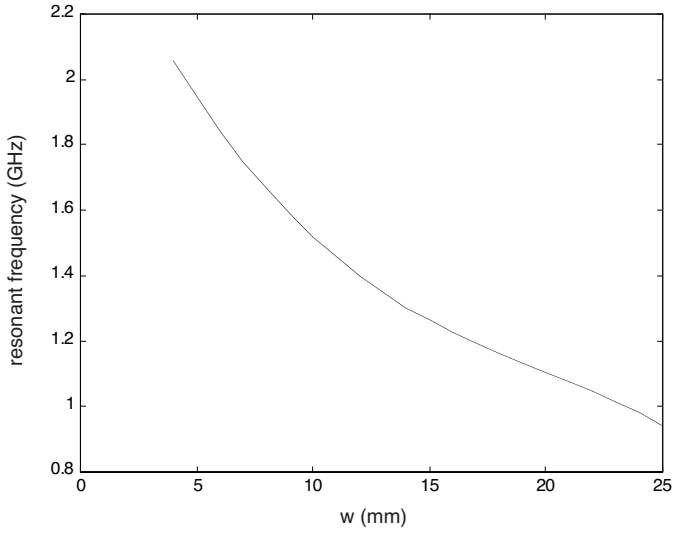

Figure 5. Variation of resonant frequency versus different values of the side strip length.

with the increase in the center strip length s. In this calculation, other parameters of the H-shaped patch antenna are fixed as: $b = 33\,\text{mm}$, $w = 14.3\,\text{mm}$, $d = 15\,\text{mm}$, $\varepsilon_r = 2.5$, $h = 1.59\,\text{mm}$. When s is 4.088 mm, it reaches 2.17 GHz; 1.59 GHz when $s = 14.99\,\text{mm}$; 1.41 GHz when $s = 20.44\,\text{mm}$; and 1.29 GHz when $s = 26\,\text{mm}$. Thus, it is shown that both the length and the width of the center strip affect the resonant frequency greatly.

The variation of resonant frequency versus different values of side strip length w is presented in Figure 5. In this calculation, other parameters of the H-shaped patch antenna are fixed as: $b = 33\,\text{mm}$, $s = 26\,\text{mm}$, $d = 15\,\text{mm}$, $\varepsilon_r = 2.5$, $h = 1.59\,\text{mm}$. The resonant frequency decreases with the increase in the side strip length w. When w is 4.769 mm, it reaches 1.97 GHz; 1.55 GHz when $w = 9.538\,\text{mm}$; 1.13 GHz when $w = 19.08\,\text{mm}$; and 0.96 GHz when $w = 24.5\,\text{mm}$. This is similar to the case in Figure 4. From the numerical results, it is interesting to find that the resonant frequency decreases more quickly with the increase in center strip lengths than that with the increase in the total of two side strip lengths ($2w$).

The characteristics of resonant frequency with respect to the side strip width b are presented in Figure 6. In this calculation, other parameters of the H-shaped patch antenna are fixed as: $w =$

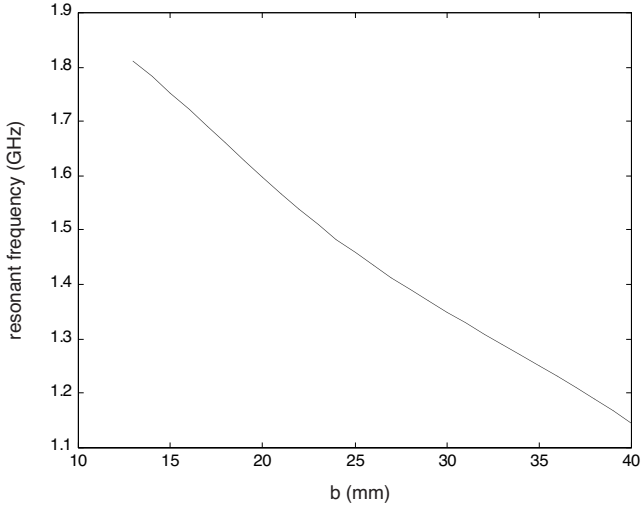

Figure 6. Variation of resonant frequency versus different values of the side strip width.

14.3 mm, $s = 26$ mm, $d = 15$ mm, $\varepsilon_r = 2.5$, $h = 1.59$ mm. The resonant frequency decreases with the increase in the side strip width b. When b is 13 mm, it reaches 1.81 GHz; 1.51 GHz when $b = 23$ mm; 1.39 GHz when $b = 28$ mm; and 1.29 GHz when $b = 33$ mm. From our numerical results, it is also found that the decrease in the side strip width b will lead to large values of resonance resistance. Actually, these observations are in accordance with previous experiences in the conventional rectangular patch antenna [4–7].

Based the results in the above figures, the design of the H-shaped patch resonant at a specific frequency can be realized by properly choosing the length and the width of the center strip and the side strip.

3.2. Electric Field and Current Distribution

To further understand the physical mechanism of the H-shaped patch antenna, it would be much helpful if we could know the electric field and current distributions. Figures 7, 8 and 9 clearly show the distributions of the electric fields E_x, E_y and E_z in the case when the parameters of the H-shaped patch antenna are $b = 33$ mm, $w = 14.3$ mm, $s = 26$ mm, $\varepsilon_r = 2.5$, $h = 1.59$ mm, and the center strip width d is changed to 2 mm, 10 mm and 33 mm, respectively. These distributions at resonance are calculated at 0.75 GHz, 1.14

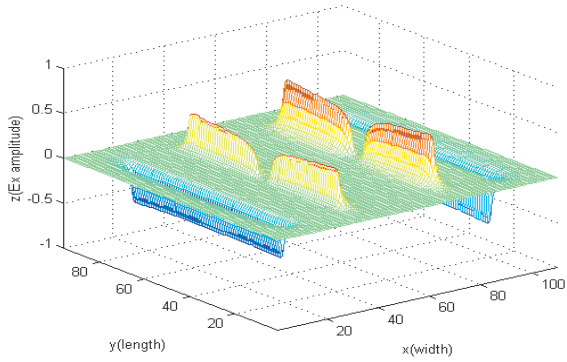

(a) E_x

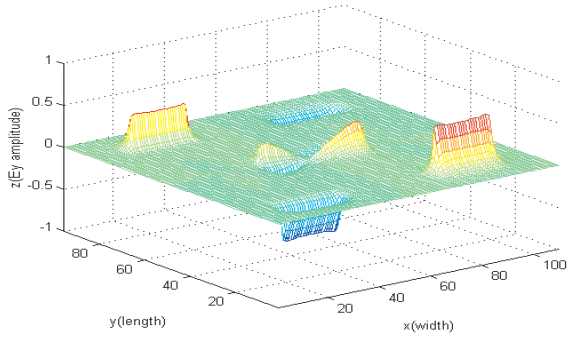

(b) E_y

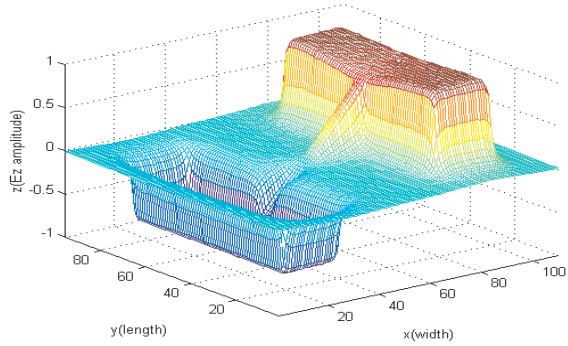

(c) E_z

Figure 7. Distributions of E_x, E_y and E_z at x-y plane, where observed plane is at the height of 1.06 mm from the ground plane ($d = 2\,\text{mm}$).

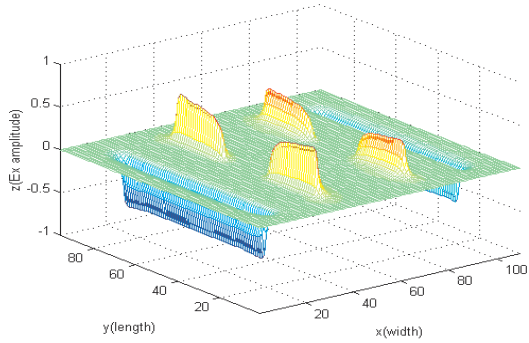

(a) E_x

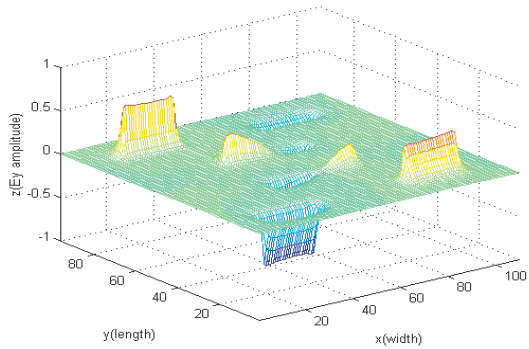

(b) E_y

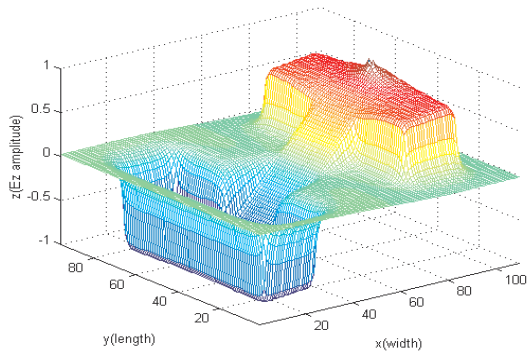

(c) E_z

Figure 8. Distributions of E_x, E_y and E_z at x-y plane, where observed plane is at the height of 1.06 mm from the ground plane ($d = 10\,\text{mm}$).

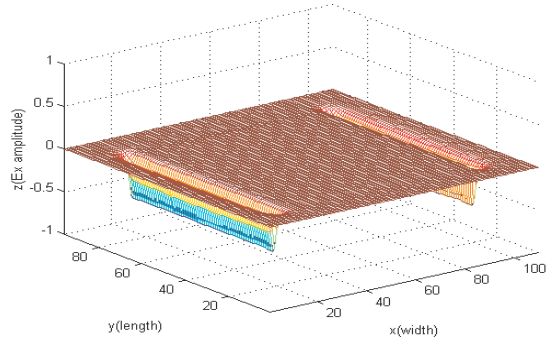

(a) E_x

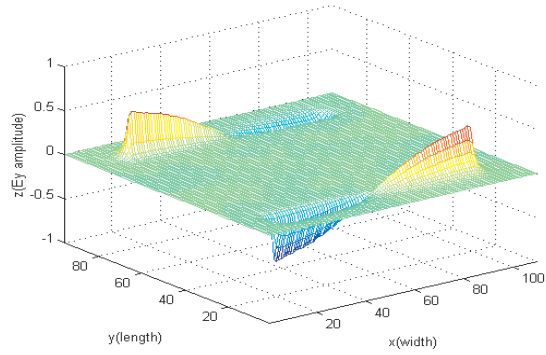

(b) E_y

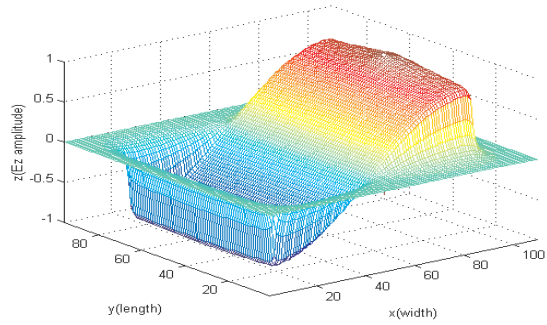

(c) E_z

Figure 9. Distributions of E_x, E_y and E_z at x-y plane, where observed plane is at the height of 1.06 mm from the ground plane ($d = 33$ mm, i.e., rectangular patch).

GHz and 1.74 GHz, respectively. In the case of $d = 33\,\text{mm}$, the distribution of the electric field E_z is found to correspond to the field distribution of TM_{100} mode of the conventional rectangular patch antenna. The distributions of electric field components E_x, E_y and E_z in the H-shaped patch are shown to be quite different from those of the conventional rectangular patch, just as expected. The distributions of electric fields also vary with the change of the center strip width. The results show that for the H-shaped patch antennas, the distribution of the electric field component E_z. is anti-symmetrical in the patch length direction (along the x axis here). The electric fields E_x, E_y and E_z. are generated at all edges of the H-shaped patch. These fringing fields are the radiating sources in the H-shaped patch antenna.

The distributions of the surface currents at resonance on both the patch and the ground plane are presented in Figures 10, 11 and 12, where the parameters of the H-shaped patch antenna are $b = 33\,\text{mm}$, $w = 14.3\,\text{mm}$, $s = 26\,\text{mm}$, $\varepsilon_r = 2.5$, $h = 1.59\,\text{mm}$, and the center strip width d is changed to 2 mm, 10 mm and 33 mm, respectively. The pointy parts of the currents in the figure correspond to the feed point. For the case of $d = 33\,\text{mm}$, the current distribution of J_x follows the well known $\sin(x)$ distribution along the x axis and approximately the $\frac{1}{\sqrt{1-y^2}}$ distribution (i.e., edge conditions) along the y axis. Compared with Figure 12, it is seen that the electric current distributions are strongly affected by the H shape. This resulted electric current distributions lead to the decrease of the resonance frequency. Very large currents J_x are shown on the H-shaped patch and ground plane; consequently, these current distributions are considered to excite the inner electric and magnetic fields between the patch and the ground plane. The current J_x of the H-shaped patch has the largest amplitude upon the center strip area, which is much narrower than the side strips. This phenomenon is physically understandable in accordance with the continuity of current. It is noted that for the H-shaped patch, the current J_x upon the center strip is non-uniform along the y axis, with the maximum values at the patch edges along y axis. The magnitude of J_x, i.e., the copolar current component, is symmetric with respect to the center point and in phase on almost the entire surface except in the vicinity of the feed point [Fig. 10(a) and Fig. 11(a)] . The magnitude of J_y, i.e., the crosspolar current component, is also symmetric with respect to the patch center, but out of phase on two sides [Fig. 10(b) and Fig. 11(b)]. It is also interesting to note that the current distributions on the ground plane seem to be just the image of the current distributions on the patch.

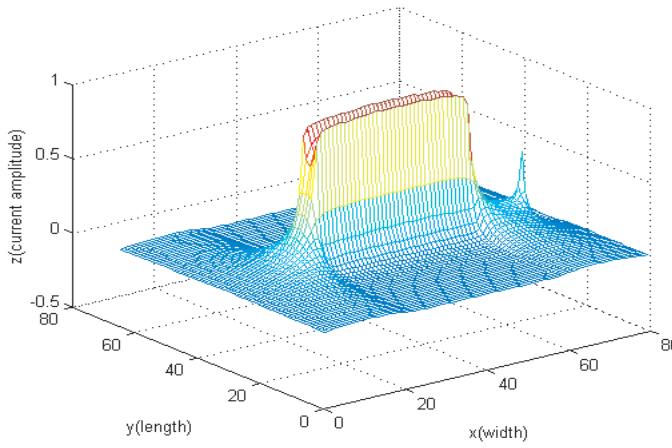

(a) J_x on patch

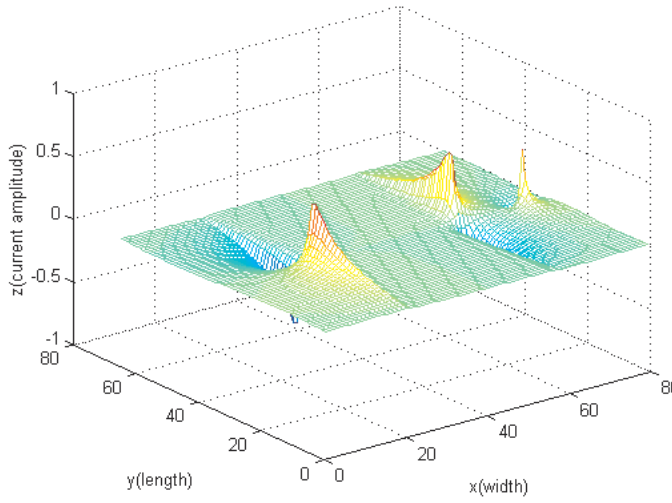

(b) J_y on patch

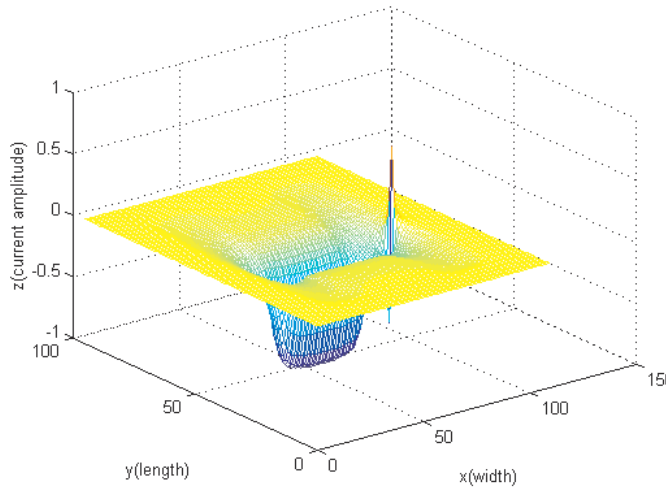

(c) J_x on ground

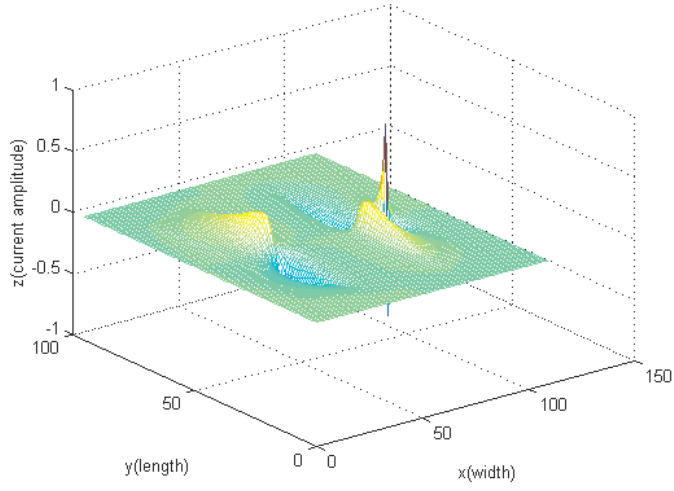

(d) J_y on ground

Figure 10. Electric current distributions on the patch and those on the ground plane ($d = 2\,\mathrm{mm}$).

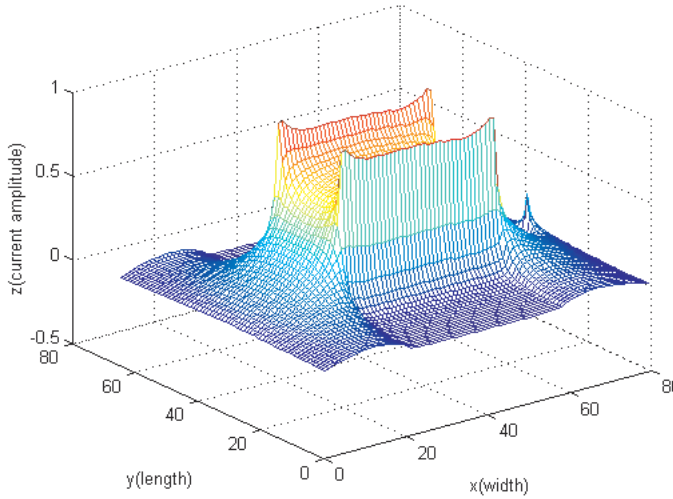

(a) J_x on ground plane

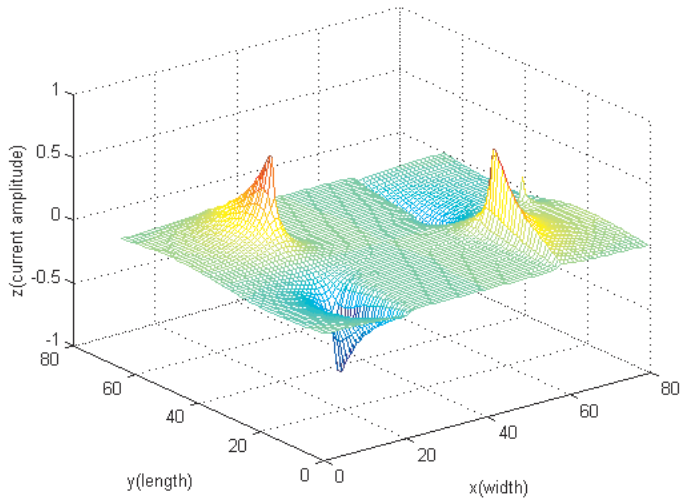

(b) J_y on ground plane

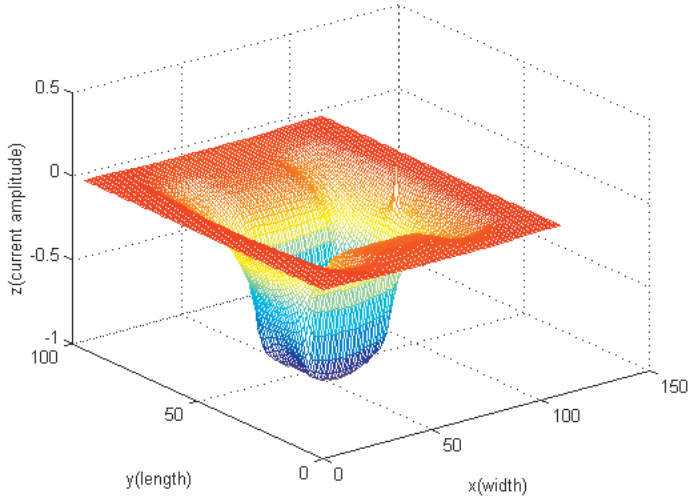

(c) J_x on ground plane

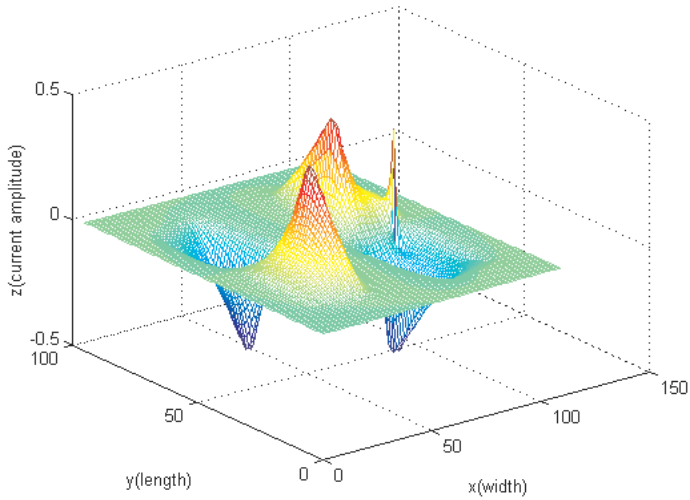

(d) J_y on ground plane

Figure 11. Electric current distributions on the patch and those on the ground plane ($d = 10\,\text{mm}$).

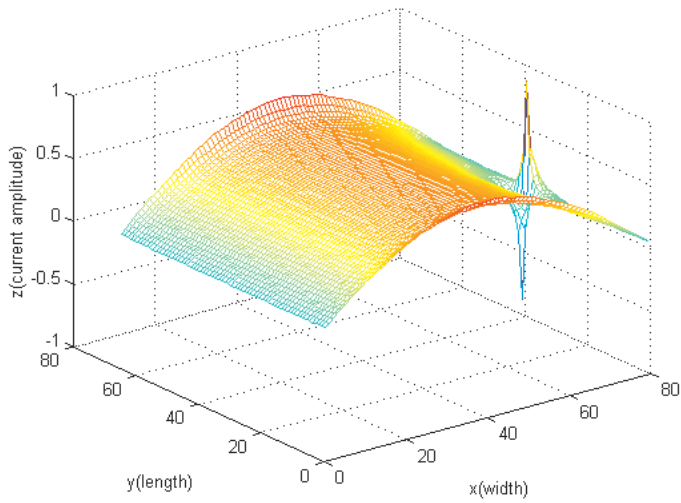

(a) J_x on ground plane

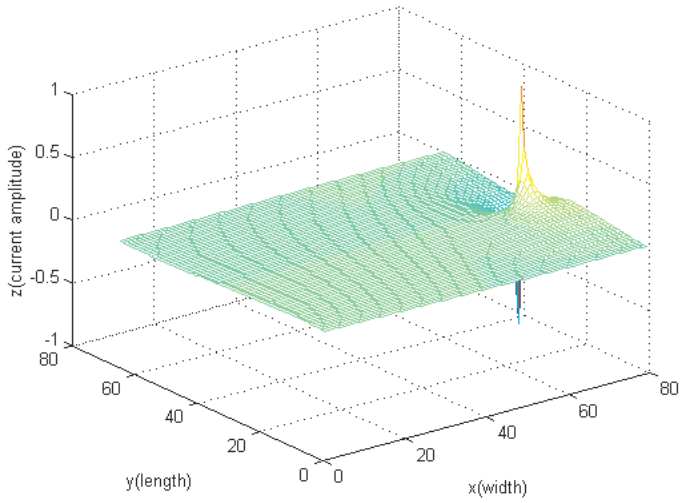

(b) J_y on ground plane

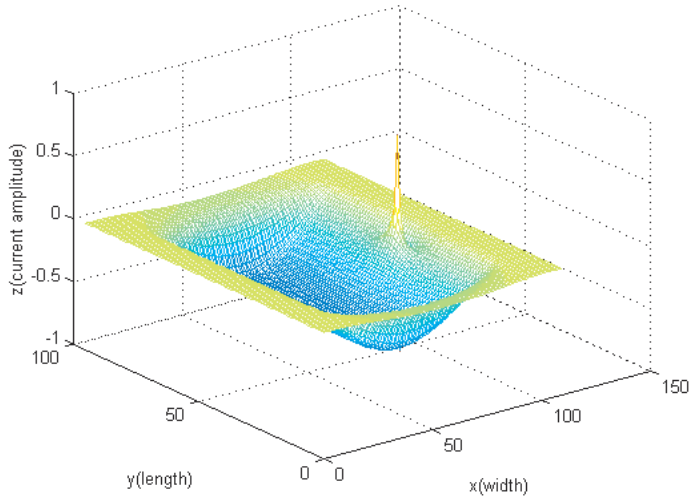

(c) J_x on ground plane

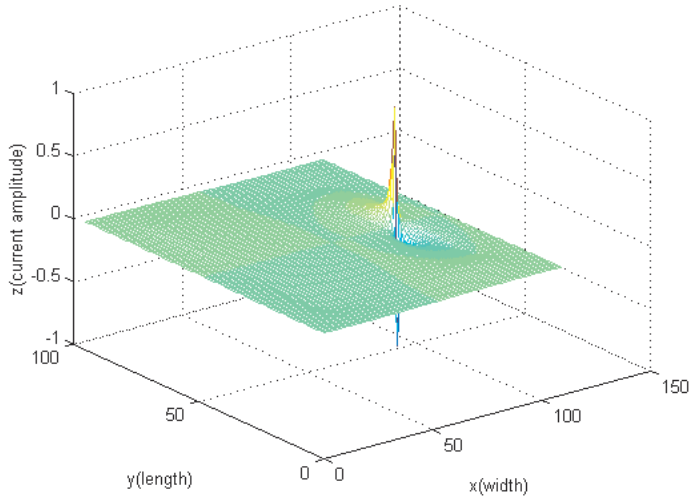

(d) J_y on ground plane

Figure 12. Electric current distributions on the patch and those on the ground plane ($d = 33\,\text{mm}$, i.e., conventional rectangular patch).

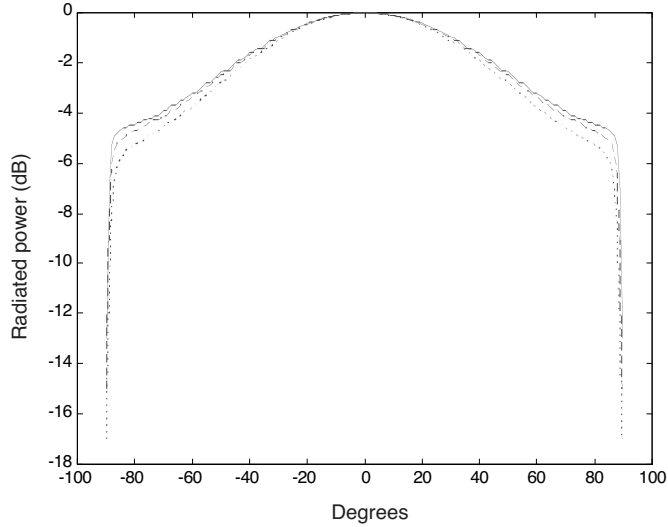

(a) E-plane pattern ($\phi = 0°$)

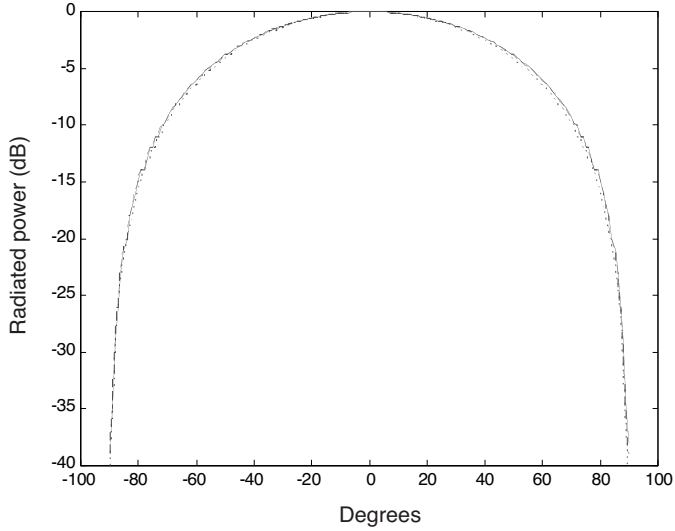

(b) H-plane pattern ($\phi = 90°$)

Figure 13. Radiation patterns $d = 2\,\text{mm}$: solid line; $d = 10\,\text{mm}$: dashed line; $d = 33\,\text{mm}$: dotted line.

3.3. Radiation Patterns

The radiation patterns of the H-shaped patches with different center strip widths are shown in Figure 13. Figure 13(a) shows the E-plane radiation patterns for the patch antenna, where the parameters of the H-shaped patch antenna are $b = 33\,\text{mm}$, $w = 14.3\,\text{mm}, s = 26\,\text{mm}$, $\varepsilon_r = 2.5$, $h = 1.59\,\text{mm}$, and the center strip width d is changed as 2 mm, 10 mm and 33 mm, respectively. These patterns are calculated at 0.75 GHz, 1.14 GHz and 1.74 GHz, respectively. It is seen that when the center strip width d decreases, the radiation patterns are broadened in the E plane. According to the numerical results, slightly broadening of radiation pattern in the H plane is also found. However, in the cases studied, the extent of broadening is so small in the H plane that they seem to coincide, as shown in the Figure 13(b). The effects of other parameters on the radiation patterns are also studied. It is found that the patterns in both the E and H planes will be broadened with the increase of center strip length s, or the decrease of side strip length w, or the decrease of side strip width b. These results are not presented for brevity.

4. CONCLUSIONS

Based on the finite-difference time-domain (FDTD) method, the characteristics of the H-shaped microstrip patch antenna are studied. Firstly, the FDTD code developed by us is verified by available measurement results. As the H-shaped patch antenna has a smaller size than those of conventional rectangular patch antenna and the ring antenna, it is very promising for many practical applications. The variations of resonant frequency with respect to different antenna parameters (including the center strip length and width, and the side strip length and width) are illustrated and discussed. It is shown that the reduction of center strip width is a very effective way of reducing the antenna size. The electric field distributions, and current distributions on both the patch and the ground plane for the H-shaped patch antenna with different center strip widths are described and presented. Finally, radiation patterns in the E- and H-planes for the H-shaped patch antenna with different center strip widths are given. It is shown that the E-plane patterns are broadened with the decrease of center strip width. Detailed numerical results are presented, which are useful for practical antenna designs. Compared with other techniques of realizing compact antennas, i.e., using high dielectric constant material [8] or adding shorting pins [9–12], the H-shaped patch antenna has advantages of low cost and ease of fabrication. Because the H-shaped patch has a small size, compact

antenna with circular polarization can also be realized by sequentially rotating of the H-shaped patch [26]. Further work is still on the way to design high performance arrays with the H-shape patch antenna.

REFERENCES

1. Ito, K., K. Ohmaru, and Y. Konishi, "Planar antennas for satellite reception," *lEEE Trans. on Broadcasting,* Vol. 34, 457–464, Dec. 1988.
2. Wu, T. K. and J. Huang, "Low-cost antennas for DBS radio," *IEEE AP-S Symp.,* 1008–1011, June 1994.
3. Henderson, A. and J. R. James, "Low-cost flate-plate array with squinted beam for DBS reception," *IEE Proc. Part. H,* Vol. 134, 509–514, 1987.
4. James, J. R. and P. S. Hall (eds.), *Handbook of Microstrip Antennas,* Peter Peregrinus, UK, 1989.
5. Gao, S.-C., L.-W. Li, T.-S. Yeo, and M.-S. Leong, "Low-cost, dual linearly-polarized microstrip patch array," *IEE Proc. Microw. Antennas Propag.,* Vol. 148, 21–25, Feb. 2001.
6. Gao, S.-C., L.-W. Li, T.-S. Yeo, and M.-S. Leong, "FDTD analysis of a slot-loaded, meandered rectangular patch antenna for dual-frequency operation," *IEE Proc. Microw. Antennas Propag.,* Vol. 148, 65–71, Feb. 2001.
7. Gao, S.-C., "Dual-polarized microstrip antenna elements and arrays for active integration," Shanghai University Press, Shanghai, P.R. China, 2000.
8. Lo, T. K., "Miniature aperture-coupled microstrip antenna of very high permittivity," *Electronics Letters,* Vol. 33, No. 1, 9–10, 1997.
9. Sanad, M., "Effects of the shorting posts on short circuit microstrip antennas," *Proc. IEEE Antenna Propagat. Symp.,* 794–797, 1994.
10. Waterhouse, R., "Small microstrip patch antenna," *Electronics Letters,* Vol. 31, No. 8, 604–605, 1995.
11. Park, I. and R. Mittra, "Aperture-coupled small microstrip antenna," *Electronics Letters,* Vol. 32, 1741–1742, Sept. 1996.
12. Waterhouse, R., "Design and performance of small printed antenna," *IEEE Trans. Antennas and Propagat.,* Vol. 46, No. 11, 1629–1633, 1998.
13. Luk, K. M., R. Chair and K. F. Lee, "Small rectangular patch antenna," *Electronics Letters,* Vol. 34, 2366–2367, 1998.
14. Chair, R., K. M. Luk and K. F. Lee, "Miniature multiplayer

shorted patch antenna," *Electronics Letters,* Vol. 36, No. 1, 3–4, 2000.

15. Wong, K. L. and S. C. Pan, "Compact triangular microstrip antenna," *Electronics Letters,* Vol. 33, No. 6, 433–434, 1997.
16. Chen, W. S., "Single-feed dual-frequency rectangular microstrip antenna with square slot," *Electronics Letters,* Vol. 34, No. 3, 231–232, 1998.
17. Gao, S.-C. and J. Li, "FDTD analysis of a size-reduced, dua-frequency patch antenna," *Progress In Electromagnetics Research,* PIER 23, 59–77, 1999.
18. Bafrooei, P. M. and L. Shafai, "Characteristics of single- and double-layer microstrip square-ring antennas," *IEEE Trans.Antennas and Propagation,* Vol. AP-47, 1633–1639, Oct. 1999.
19. Palanisamy, V. and R. Garg, "Rectangular ring and H-shaped microstrip antennas — 'Alternatives to rectangular patch antenna'," *Electronics Letters,* Vol. 21, No. 19, 874–876, 1985.
20. Yee, K. S., "Numerical solution of initial boundary value problems involving Maxwell's equations in isotropic media," *IEEE Trans. Antennas and Propagation,* Vol. AP-14, 302–307, May 1966.
21. Liao, Z. P., H. L. Wong, G. P. Yang, and Y. F. Yuan, "A transmitting boundary for transient wave analysis," *Scientia Sinica,* Vol. 28, No. 10, 1063–1076, Oct. 1984.
22. Mei, K. K. and J. Fang, "Superabsorption — a method to improve absorbing boundary conditions," *IEEE Trans. Antennas and Propagation,* Vol. AP-40, 1001–1010, Sept. 1992.
23. Gao, S.-C. and J. Li, "FDTD analysis of serial corner-fed square patch antennas for single- and dual-polarized applications," *IEE Proc. Microw. Antennas Propag.,* Vol. 146, 205–209, June 1999.
24. Gupta, K. C. and P. S. Hall (eds.), *Analysis and Design of Integrated Circuit-Antenna Modules,* John Wiley & Sons, Inc., New York, 2000.
25. Wu, S. C., N. G. Alexopoulos, and O. Fordham, "Feeding structure contribution to radiation by patch antennas with rectangular boundaries," *IEEE Trans. Antennas and Propagation,* Vol. AP-40, 1245–1250, Oct. 1992.
26. Huang, J., "Techniques for an array to generate circular polarization with linearly polarization with linearly polarized elements," *IEEE Trans. Antennas and Propagation,* Vol. AP-34, 1113–1123, Sept. 1986.